Original Article
Gastrodia elata Blume (tianma) mobilizes neuro-protective capacities

Arulmani Manavalan[1,2], Umamaheswari Ramachandran[1,2], Husvinee Sundaramurthi[1], Manisha Mishra[1,2], Siu Kwan Sze[1], Jiang-Miao Hu[3], Zhi Wei Feng[1], Klaus Heese[1,2]

[1]School of Biological Sciences, College of Science, Nanyang Technological University, 60 Nanyang Drive, Singapore 637551, Singapore; [2]Institute of Advanced Studies, Nanyang Technological University, 60 Nanyang View, Singapore 639673, Singapore; [3]Kunming Institute of Botany, Chinese Academy of Science, Kunming, Yunnan 650204, People's Republic of China.

Abstract: Tianma (*Gastrodia elata Blume*) is a traditional Chinese medicine (TCM) often used for the treatment of headache, convulsions, hypertension and neurodegenerative diseases. Tianma also modulates the cleavage of the amyloid precursor protein App and cognitive functions in mice. The neuronal actions of tianma thus led us to investigate its specific effects on neuronal signalling. Accordingly, this pilot study was designed to examine the effects of tianma on the proteome metabolism in differentiated mouse neuronal N2a cells using an iTRAQ (isobaric tags for relative and absolute quantitation)-based proteomics research approach. We identified 2178 proteins, out of which 74 were found to be altered upon tianma treatment in differentiated mouse neuronal N2a cells. Based on the observed data obtained, we hypothesize that tianma could promote neuro-regenerative processes by inhibiting stress-related proteins and mobilizing neuroprotective genes such as Nxn, Dbnl, Mobkl3, Clic4, Mki67 and Bax with various regenerative modalities and capacities related to neuro-synaptic plasticity.

Keywords: Aging, tianma, neuron, neurodegeneration, metabolism, signalling, TCM

Introduction

Since recent data show that the number of people affected by Alzheimer's disease (AD) and dementia is increasing at an epidemic pace, there has been a interest in developing novel protective agents because biological aging also represents the major risk factor with respect to the development of AD, vascular dementia (VD) and other cardiovascular diseases (CD). Traditional herbal medicine is especially attractive for disease prevention, health maintenance, and sicknesses that are non-responsive to current Western medicine and thus has potential benefits that attract worldwide attention and interests. The use of medicinal herbs has a long history in Asia and is commonly used to treat various neurological diseases including stroke, epilepsy and VD [1-3]. Orchids and their derivatives have been shown to benefit the improvement of neural functions in clinical studies but the underlying mechanisms are largely unknown which severely hampered the more extensive applica-

tion of such potential drugs as well as the potential of industrial exploitation of it [4-6]. According to ancient Chinese medical literature, tianma (*Gastrodia elata Blume,* Orchidaceae) is a herbal medicine for the control of the internal movement of wind. The dry tuber of tianma has long been officially listed in the Chinese Pharmacopoeia and is used in treating headaches, dizziness, tetanus, epilepsy, infantile convulsions and numbness of the limbs [4, 6-11]. Previously, we could demonstrate *in vivo* the potential neuro-protective action of tianma and its capacity to enhance cognitive functions in mice [12].

Recently, we have successfully applied the two dimensional (2D) liquid chromatography coupled with tandem mass spectrometry-based isobaric tag for relative and absolute quantification (2D-LC-MS/MS-iTRAQ) strategy in the area of neuro-degenerative diseases [13, 14]. Our group has recently reported the facilitating effect of tianma on α-secretase-mediated cleav-

age of the amyloid precursor protein (App) towards a non-amyloidogenic pathway and on cognitive functions in mice [12]. We used here the proteomics approach in our mouse neural N2a cell model for quantitative profiling of tianma-regulated genes. In quest of the metabolic changes in the entire mouse neuronal proteome, the iTRAQ-based proteomics-bioinformatics platform was applied to generate a list of proteins comprising the regulated proteins from differentiated mouse neuronal N2a cells stimulated by tianma. Finally, some of the regulated proteins were validated at the protein levels by western blot analyses to prove their neural regulation upon tianma stimulation (**Figure 1**). Our *in vitro* results show the effect of tianma on mouse neural cell proteome changes and its potential implication for possible therapeutic neuro-regenerative applications. Since tianma is a novel potential neuro-protective herb with many unidentified features, our present investigation could further contribute to its operational assignment on neurons to unravel the mysteries behind the neuro-protective activities of tianma.

Materials and methods

Reagents

Unless indicated, all reagents used for biochemical methods were purchased from Sigma-Aldrich (St. Louis, MO, USA). Materials and reagents for SDS-PAGE (sodium dodecyl sulfate-polyacrylamide gel electrophoresis) were from Bio-Rad (Bio-Rad Laboratories, Hercules, CA, USA). The iTRAQ reagent multi-plex kit was bought commercially (Applied Biosystems, Foster City, CA, USA).

Antibodies

Anti-Calr (Calreticulin, 1:1000, rabbit polyclonal; Abcam, Cambridge, UK), anti-Clic4 (Chloride intracellular channel 4 (mitochondrial (mt)), 1:500, goat polyclonal; Abcam), anti-Gapdh (Glyceraldehyde-3-phosphate dehydrogenase, 1:1000, mouse monoclonal; Santa Cruz Biotechnology Inc., Santa Cruz, CA, USA), anti-H2afj (H2A histone family, member J, 1:800, rabbit polyclonal; Novus Biologicals, LLC, Littleton, CO, USA), anti-Hnrnpu (heterogeneous nuclear ribonucleoprotein U, 1:1000, mouse monoclonal; Abcam), anti-Hspa5 (heat shock protein 5, 1:1000, rabbit polyclonal; Abnova, Taipei City,

Taiwan), anti-Hsp90α (heat shock protein 90α, 1:1000, mouse monoclonal; Santa Cruz), anti-Vimentin (V9) (1:1000, mouse monoclonal; Lab Vision Products, Thermo Fisher Scientific Inc., Fremont, CA, USA), anti-Sept2 (Septin 2, 1:200, goat polyclonal; Santa Cruz), anti-Trim28 (tripartite motif-containing 28, also Tif1b (Transcriptional intermediary factor 1 beta), 1:600; rabbit polyclonal, Santa Cruz).

Tianma preparation

The rhizome of *Gastrodia elata* (tianma), grown under standardized conditions [15], was collected from Zhaotong City, China and was provided by Dr. Jun Zhou (Kunming Institute of Botany, Chinese Academy of Science, Yunnan, People's Republic of China). The species was identified and chemically analyzed as reported previously [12, 16]. A voucher specimen (0249742) was deposited in the herbarium of the Kunming Institute of Botany, (Chinese Academy of Science, Yunnan, P.R. China). After tianma was dissolved (0.36 g of powdered tianma in 3.6 ml deionized water) in deionized water to yield a stock solution containing a concentration of 100 mg/ml, the stock solution suspension was boiled and, at regular intervals, mixed using the thermomixer comfort (Eppendorf, Hamburg, Germany) for 1h; this stock solution was used for further procedures and the calculation of the final tianma concentration for neuronal N2a cell stimulation experiments. Following this, the mixture was centrifuged at 16,000 x g at 25 °C for 10 min. The supernatant was collected and filtered through a syringe-filter with a pore size of 0.25 µm (Acrodisc® membrane filter, Pall Corporation, Singapore) [12].

Cell culture

Mouse neuronal N2a cells (American Type Culture Collection (ATCC), Manassas, VA, USA) were propagated at 37 °C in humidified 5% CO_2/95% air, in Dulbecco's Modified Eagle's Medium (DMEM, GlutaMax™; Invitrogen) supplemented with 10 % fetal bovine serum (FBS, Invitrogen), non-essential amino acids (Invitrogen), and antibiotic-antimycotic (Invitrogen).

Tianma stimulation

N2a cells were seeded in Poly-D-Lysine (PDL)-coated six-well plates (Becton Dickinson, San Jose, CA, USA) at about 20 % confluency per
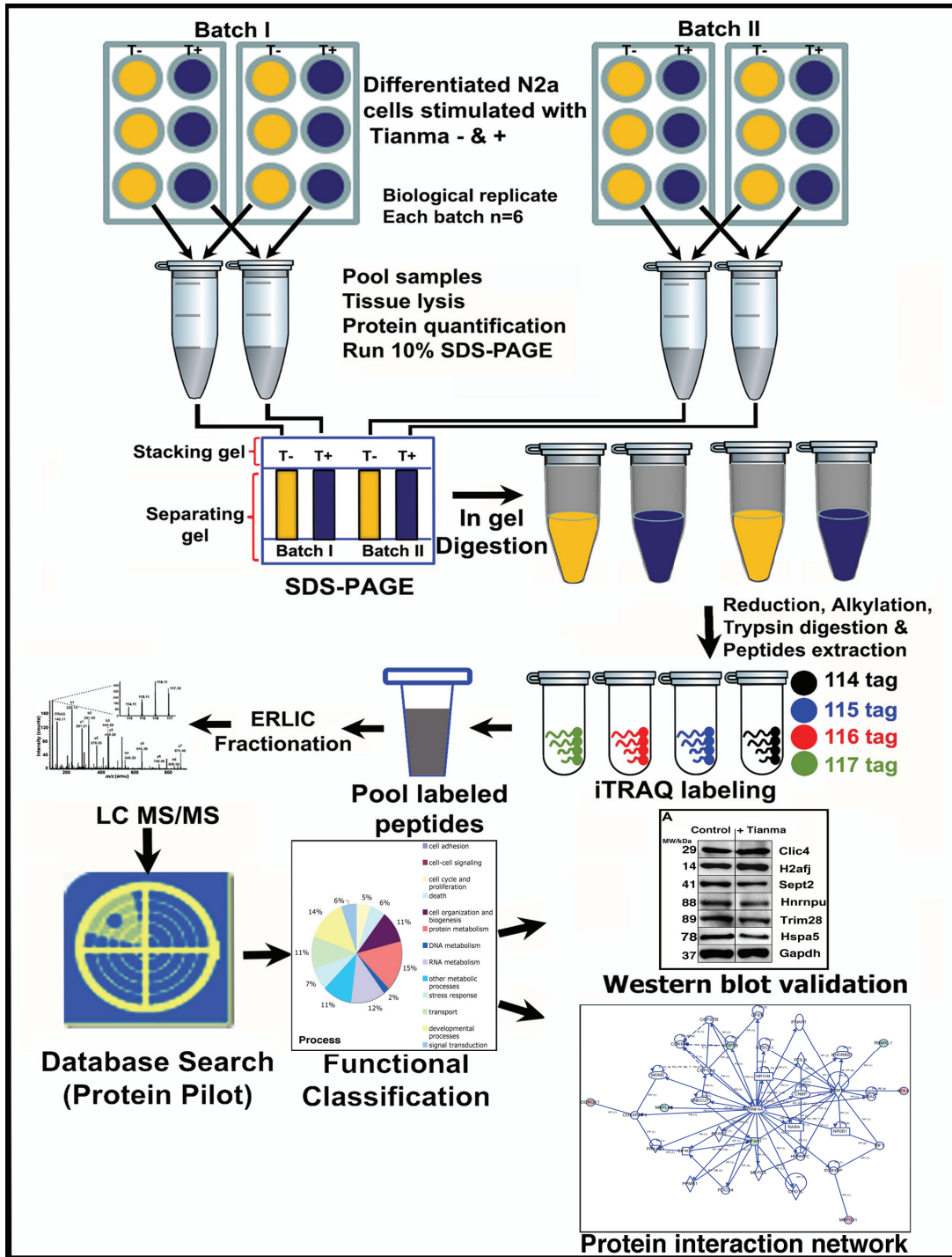
Figure 1. Schematic representation of the experimental design showing biological and technical replicates. Following differentiated mouse neuronal N2a cell lysis, protein extracts were acetone precipitated and quantified. These were then run in SDS-PAGE and subsequently in-gel digested. The quantitative proteomics analyses of each digested peptides was performed by labeling with multi-plex isobaric tags (114, 115, 116 and 117) for relative and absolute quantification (iTRAQ) reagent followed by Electrostatic Repulsion-Hydrophilic Interaction Chromatography (ERLIC)-based fractionation, and liquid chromatography coupled with tandem mass spectrometry (LC-MS/MS)-based multidimensional protein identification technology. The obtained data was analyzed using ProteinPilot software and validated by quantitative western blots. Finally, proteins were functionally classified into various subgroups.

well. Experiments were performed twice, with each set repeated six times. The cells were allowed to attach and divide for 20 hrs, after which 20 μM RA (retinoic acid) was added to 4 % FBS-containing media in all experimental plates to promote neuronal differentiation. The media was changed once every three days and images were captured via an inverted microscope (Nikon Eclipse TE2000, Chiyoda-ku, Tokyo, Japan) every 24 hrs for seven days. On the start of the eighth (8th) day post differentiation in culture, N2a cells were stimulated with tianma (without FBS, without RA) to a final concentration of 1 mg/ml per well, according to previous reports [12, 17], for 30 hrs (control cells received mock-treatment with the solvent only) and subsequently, images were captured before proceeding with cell lysis.

Cell lysate preparation

All steps were performed on ice. Cell lysis buffer (ice-cold) was prepared with 2 % SDS, 0.5 M Triethyl ammonium bicarbonate buffer (TEAB), 1 Complete™ protease inhibitor cocktail tablet (Roche, Mannheim, Germany) and 1 PhosSTOP phosphatase inhibitor cocktail tablet (Roche). The wells were washed with ice-cold phosphate buffered saline (PBS) twice to remove debris and dead cells. 100 μl of cell lysis buffer was added to each well and using a cell scraper (Greiner Bio-One GmbH, Frickenhausen, Germany), the attached cells were collected (six wells with same experimental conditions were pooled). The pooled cell lysate was subjected to a quick spin and sonicated for 1 min (Vibra Cell™ ultrasonic processor, Jencon, Leighton Buzzard, Bedfordshire, UK) at an amplitude of 30 Watt and a pulse (3 sec on and 6 sec off). The cell lysate samples were centrifuged at 16,000 x g at 4 °C for 1 hr, supernatant was collected and stored at -20 °C until further use. The protein concentration was quantified by a '2-D Quant' kit (Amersham, Piscataway, NJ, USA) according to the manufacturer's protocol.

iTRAQ protocol

The 2D-LC-MS/MS-iTRAQ procedures were performed as described previously [13, 14, 17, 18]. The detailed protocols including post-proteomic data verification by SDS-PAGE, western blot [19-21] are presented as the following for readers' convenience.

Sample preparation - acetone precipitation:

Each sample condition had 600 μg of total protein lysate transferred to a new tube. Six volumes of 100 % -20 °C-chilled acetone were added to each tube and vortexed thoroughly at regular intervals. The tubes were incubated overnight at -20 °C and the following day, vortexed and centrifuged at 16,000 x g for 30 min to pellet down all proteins. The supernatant was discarded and the pellets were disturbed and washed in 500 μl of 90 % -20 °C-chilled acetone. Subsequently, the tubes were centrifuged at 16,000 x g for 20 min and the supernatant discarded. The washed pellets were allowed to air-dry at room temperature (RT) for 15 min, then dissolved in 100 μl of 200 mM TEAB and 2 % SDS and incubated at 50 °C for 5-10 min with simple agitation using a thermomixer (Eppendorf, Hamburg, Germany). Following which the tubes were centrifuged at 16,000 x g for 30 min. The supernatant was collected and protein concentration re-quantified using the '2-D Quant' kit (Amersham).

SDS-PAGE and in-gel digestion: Each sample had 200 μg of acetone-precipitated proteins prepared (mixed with loading dye), denatured for 10 min in a thermo bath (Fine PCR, Seoul, Korea) and resolved up to 60 %. The gels were washed twice with autoclaved Milli-Q Water (MQW) for 5 min each. Fixing solution (50 % methanol and 10 % Acetic Acid (AcOH)) was added till the gels were submerged and kept overnight on a SH30L reciprocating shaker (Fine PCR). The gels were then washed with MQW thrice for 15 min each. In-gel digestion was performed in a laminar flow hood (Gelman, Singapore). The gels were diced into 1 – 2 mm pieces and transferred into tubes. 5 ml of 25 mM TEAB in 50 % Acetonitrile (ACN) buffer was added to the tubes, vortexed and left at RT for 10 min after which the buffer was discarded and the step repeated four times. Finally, 80 % ACN in 20 mM TEAB was added, vortexed and the tubes were left at RT for 10 min. The supernatant was discarded and the sample tubes were left to air-dry for 30 min.

Reduction, alkylation, trypsin digestion and extraction: Stock solutions of 200 mM tris (2-carboxyethyl) phosphine (TCEP) in HPLC water (J.T. Baker, Mallinckrodt, Inc., Phillipsburg, NJ, USA) and 200 mM S-methyl methanethiosulfonate (MMTS) in isopropanol were prepared. 5 mM of TCEP in 25 mM TEAB buffer was added to the dried gel pieces, vortexed and briefly spun before being incubated at 65 °C for 1 hr

to allow a reduction reaction to take place. Following this, 10 mM MMTS in 25 mM TEAB buffer (tube was covered with aluminum foil) was added to gel pieces, vortexed and briefly spun. The alkylation reaction was then allowed to proceed for 45 min in the dark at RT. The supernatant was removed and discarded. The gel pieces were again washed with 25 mM TEAB in 50 % ACN buffer as described above. The gel was dehydrated by 100 % ACN. Finally, the tubes were air-dried for 30 min. First, 10 ml of 2.5 µg of trypsin in 25 mM TEAB buffer was added to each sample and incubated at 4 °C for 15 min for proper rehydration. Then 10 ml of 2.5 µg trypsin solution was again added to tubes and incubated overnight in a 37 °C incubator. Subsequently, the tubes were spun briefly and the aqueous extract of the digested solution was collected. To the remaining gel pieces, 50 % ACN and 1 % AcOH was added, vortexed and incubated in a water bath sonicator for 30 min. The supernatant was transferred and combined to the main sample tube. The extraction step was repeated 5 times. The trypsin digested peptides were pooled and dried completely in the SpeedVac (Concentrator 5301, Eppendorf) at 30 °C and stored at -20 °C.

Labeling of peptides with iTRAQ tags (4 plex): Each iTRAQ reagent tubes (tags- 114,115,116, 117) had 70 µl of 100 % ethanol added and vortexed thoroughly. The dried peptides were dissolved in 30 µl of 500 mM TEAB (dissolution buffer). Each iTRAQ tag was transferred to the respective peptide tubes and the tubes were incubated at RT for 2 hr with gentle shaking (thermomixer). All samples were then combined and kept in the SpeedVac at 30 °C to dry completely.

Desalting: The dried peptide samples were reconstituted in 500 µl of 0.1 % formic acid (FA) and kept in the water bath sonicator for 5 min. 50 mg C18 cartridge (Sep-Pak® Vac C18 cartridges, Waters, Milford, MA) was conditioned thrice with 100 % methanol pushed through at a rate of 2 to 3 drops per second via a syringe. The stationary phase was acidified three times with 0.1 % FA (following the same method as conditioning). The samples were loaded into the columns and allowed to flow via gravitational force and the flow-through was reloaded three times. Next, the sample loaded columns were desalted twice with 0.1 % FA. Elution buffer (75 % ACN + 0.1 % FA) was added and, using a sy-

ringe, the buffer was pushed through the columns and the samples were collected. This C18 desalting protocol was performed thrice with the desalting wash's solution and the flow-through combined together. The samples were pooled and placed in the SpeedVac to dry and stored at -20 °C.

Electrostatic repulsion-hydrophilic interaction chromatography (ERLIC): Eight hundred µg of iTRAQ-labeled peptides were fractionated using PolyWAX LP weak anion-exchange column (4.6 × 200 mm, 5 µm, 300 Å; PolyLC, Columbia, MD, USA), within the Shimadzu HPLC system (Kyoto, Japan). The HPLC gradient used composed of 100 % solvent A (85 % ACN, 0.1 % AcOH, 10 mM ammonium acetate, 1 % FA, pH 3.5) for 5 min, 0 %–36 % solvent B (30 % ACN, 0.1 % FA, pH 3.0) for 15 min, and 36 %–100 % solvent B for 25 min, and finally 100 % solvent B for 10 min, running for a total of 1 hr at a flow rate of 1.0 ml min^{-1}. A total of 29 fractions were collected and was later reduced to 16 fractions by pooling of samples. The 16 sample tubes were kept in SpeedVac to dry completely. The dried peptides in each sample tube were reconstituted in 100 µl 0.1 % FA for LC-MS/MS analysis.

LC-MS/MS analysis: The samples were analyzed thrice (technical replicate = 3) for LC-MS/MS using a Q-Star Elite mass spectrometer (Applied Biosystems/MDS SCIEX) coupled with an online microflow HPLC system (Shimadzu). 30 µL of peptide mixture was injected and separated on a home-packed nanobored C18 column with a picofrit nanospray tip (75 µm i.d. × 15 cm, 5 µm particles) (New Objectives, Wubrun, MA, USA) for each analysis (Multiple injections give a better coverage of the target proteome with superior statistical consistency. This is especially true for single peptide proteins as more MS/MS spectral evidence was obtained from multiple injections leading to higher confidence of peptide identification and quantification.). The samples were separated at a constant flow rate of 30 µL/min with a splitter achieving an effective flow rate of 0.3 µL/min. Data acquisition was performed in the positive ion mode, with a selected mass range of 300-1600 m/z, and peptide ions with +2 to +4 charge states were subject to MS/MS. The three most abundant peptide ions above 5 count threshold were selected for MS/MS and each selected target ion was dynamically excluded for 30 s with 30 mDa mass tolerance. Automatic collision energy and

automatic MS/MS accumulation were used to activate smart information-dependent acquisition (IDA). With maximum accumulation time being 2 s, the fragment intensity multiplier was set to 20. The relative abundance of the proteins in the samples was reflected by the peak areas of the iTRAQ reporter ions.

Mass spectrometric data analysis: The data was acquired with the Analyst QS 2.0 software (Applied Biosystems/MDS SCIEX). Using Protein-Pilot Software 3.0, Revision Number: 114732 (Applied Biosystems), protein identification and quantification were performed. The peptides were identified by the Paragon algorithm in the ProteinPilot software and the differences between expressions of various isoforms were traced by Pro Group algorithm using isoform-specific quantification. The parameters used for database search were defined as follows: (i) Sample Type: iTRAQ 4plex (Peptide Labeled); (ii) Cysteine alkylation: MMTS; (iii) Digestion: Trypsin; (iv) Instrument: QSTAR Elite ESI; (v) Special factors: None; (vi) Species: None; (vii) Specify Processing: Quantitate; (viii) ID Focus: biological modifications, amino acid substitutions; (ix) Database: concatenated 'target' (International Protein Index (IPI) mouse; version 3.55; 55,956 sequences) and 'decoy' (the corresponding reverse sequences for false discovery rate (FDR) estimation); (x) Search effort: thorough. Pro Group algorithm was used to automatically select the peptide for iTRAQ quantification, where the reporter peak area, error factor (EF) and p value were calculated. Auto bias-correction was carried out on the acquired data to remove variations imparted as a result of unequal mixing during the combination of the differently labeled samples. To minimize the false positive identification of proteins, a strict cut-off of unused ProtScore $\geq$ 2 was used as the qualification criteria, which corresponds to a peptide confidence level of 99 %. A FDR of 0.33 % (<1.0 %) was applied. The cut-off for up- or down-regulation (pre-defined at 1.2 and 0.83 respectively) was determined by using the *p*-value cut-off (0.05) to obtain the list of proteins with significant ratios. The *p*-value assigned by the ProteinPilot software measures the confidence of the real change in the protein expression level. Furthermore, the mean values plus standard deviation values were obtained from the iTRAQ ratios for batches, B-I and B-II. Data analysis and functional classification were conducted using online databases such as NCBI, UniProt, and Panther.

Post-proteomic data verification by SDS-PAGE and western blot analysis: The same pooled extracts were used for post-proteomics data validation using western blot analysis. Twenty micrograms of cell lysates were resolved by 8-12 % SDS-PAGE at 0.02 Ampere (A) of constant current and transferred to a polyvinylidine fluoride (PVDF) membrane (0.22 µm; Amersham) using the 'semi-dry' transfer method (BioRad, Singapore) for 60 min at 0.12 A in buffer containing 25 mM Tris, 192 mM glycine, 20 % methanol, and 0.01 % (wt/vol) SDS. The membrane was blocked with 5 % BSA (bovine serum albumin; BioRad) in Phosphate-buffered saline (PBS) plus 0.1 % Tween-20 (PBS-T) for 2 hrs at RT, washed three times in PBS-T for 10 min each, and incubated with primary antibody (diluted in 2 % BSA in PBS-T) for overnight at 4 ° C. The membranes were washed as described above, incubated with HRP-conjugated secondary antibody for 1 hr at RT, and developed using the ECL plus western blot detection reagent (Amersham). X-ray films (Konica Minolta Inc., Tokyo, Japan) were exposed to the membranes before film development in a Kodak X-OMAT 2000 processor (Kodak, Ontario, Canada). For equal sample loading, protein concentration was quantified with '2D Quant' kit (Amersham) with at least two independent replicates. BSA was used as the standard. To re-probe the same membrane with another primary antibody, Pierce's (Pierce Biotechnology, Inc., Rockford, IL, USA) 'stripping solution' was used to strip the membranes. In addition, equal sample loading was confirmed using Gapdh as a reference protein. Western blot experiments were performed at least three times for statistical quantification and analyses (n = 3), and representative blots are shown. Values (= relative protein expression) represent the ratio of densitometric scores (GS-800 Calibrated Densitometer and Quantity One quantification analysis software version 4.5.2; BioRad) for the respective western-blot products (mean ± SD (standard deviation)) using the Gapdh bands as a reference for loading control.

Statistical analysis

The data obtained in the western blot analyses in this investigation are illustrated as mean ± SD. Student's *t*-test was performed. For the iTRAQ analysis ProteinPilot Software 3.0 was
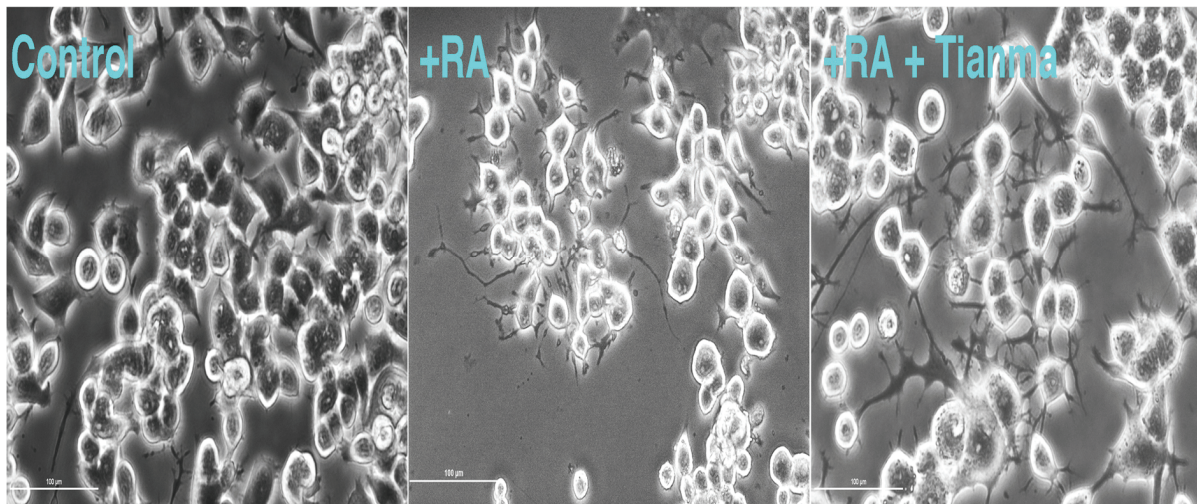
Figure 2. Mouse neuronal N2a cells were seeded and cultured in PDL-coated six well plates. Control cells were cultured in 10 % FBS. RA-treated cells were grown in the presence of 4 % FBS and 20 µM retinoic acid (RA) for 7 days for differentiation. RA+tianma-treated cells were grown in the presence of 4 % FBS and 20 µM RA for 7 days for differentiation before tianma stimulation was induced on the 8th day (adding 1 mg/ml tianma for 30 hrs; without FBS, without RA) as described in material and methods (controls and RA-treated cells received a mock-treatment with the solvent only). Representative images show that RA induced neurite outgrowth. These images show that the stimulation of neuronal N2a cells with tianma resulted in slightly enhanced neurite extensions. Scale-bar = 100 µm.

used as described in the experimental procedures.

Results

All experiments were performed twice (B-I and B-II; **Figure 1**) with each set repeated six times (six controls and six tianma-treated cells for B-I and B-II, respectively). We used four samples to perform iTRAQ (two controls (B-I+B-II) and two tianma-activated (B-I + B-II) samples; with each sample as six pooled biological replicates (**Figure 1**)). This was to ensure high confidence in the detection of tianma-regulated proteins. The quality of the dataset and instrumental reproducibility was then confirmed by comparing and combining three technical replicates [13] after the labelling of the peptide solutions from different samples with 114, 115, 116 and 117 isobaric tags and processed in LC-MS/MS.

The morphological effect of tianma on differentiated neuronal N2a cells

Upon tianma stimulation of differentiated neuronal N2a cells, the neurite outgrowth was slightly enhanced but insignificant between control (RA-treated) and tianma-treated cells (**Figure 2**).

Identification of proteins in differentiated neuronal N2a cells activated by tianma

Through iTRAQ, we identified a total of 2178 proteins, out of which 699 showed an altered protein expression level, and we finally obtained 74 proteins (**Table 1**) that exhibited common trends in both experimental batches.

In order to verify that the protein samples were indeed from the whole mouse neuronal N2a cell proteome, the identified protein names were uploaded into JVirGel, a database software that creates a virtual 2D gel picture [22]. The proteins were categorized based on their isoelectric points and molecular weights (**Figure 3**). The virtual 2D gel image revealed well dispersed proteome, hence confirming that the samples collected originated from the whole cell proteome.

While comparing the proteins from the two batches, B-I and B-II of experiments, we found a total of 74 proteins that were significantly deregulated with the same tendency in both experimental batches B-I and B-II (**Table 1**). Essentially, 21 of these proteins were up-regulated (e.g.: Prss2) and the remaining 53 proteins were down-regulated (e.g.: Trim28, Enah, Top2a, and

Table 1. Functional classification of differentially expressed proteins between control and tianma-treated differentiated mouse neuronal N2a cells quantified by iTRAQ proteomics

Protein IDs	Gene symbols	Protein Names	Molecular Function	No. of peptides (>95%) *	T : C iTRAQ ratio	Sub-cellular location	Standard deviation
Huntington disease							
IPI00126072	Vat1	Synaptic vesicle membrane protein VAT-1 homolog	Oxidoreductase activity	20	0.54	Cytoplasm	0.1428
Parkinson disease							
IPI00114945	Sept2	Septin-2	GTPase activity	11	0.64	Cytoplasm, Cytoskeleton	0.1229
Wnt signalling pathway							
IPI00121270	Smarcd1	SWI/SNF-related matrix-associated actin-dependent regulator of chromatin subfamily D member 1	Nucleic acid binding	4	1.51	Nucleus	0.2043
Apoptosis signalling pathway							
IPI00120684	Bax	Bcl2-associated X protein	Apoptosis regulator	6	1.49	Endoplasmic reticulum	0.1864
Integrin signalling pathway							
IPI00121430	Col12a1	Collagen alpha-1 (XII) chain	Receptor activity	1	1.30	Extracellular matrix secreted	0.0576
Chaperonic response							
IPI00330804	Hsp90aa1	Heat shock protein HSP 90-alpha	ATP binding	119	0.73	Cytosol, melanosome	0.0398
IPI00229080	Hsp90ab1	Hsp90ab1 protein	ATP binding	213	0.46	Mitochondrion	0.0821
IPI00331556	Hspa4	Heat shock 70 kDa protein 4, 70-kDa heat shock cognate protein	ATP binding	53	0.53	Cytoplasm	0.1307
IPI00319992	Hspa5	78 kDa glucose-regulated protein	ATP binding	98	0.37	Endoplasmic reticulum	0.1367
IPI00116279	Cct5	T-complex protein 1 subunit epsilon	ATP binding	47	0.74	Cytoplasm, Cytoskeleton	0.0097
IPI00119618	Canx	Calnexin	Calcium ion binding	23	0.68	Endoplasmic reticulum	0.0181
GTPase activity/G-protein/Kinases							
IPI00470077	Enah	Protein enabled homolog	Structural constituent of cytoskeleton	9	0.48	Cytosol	0.1014
IPI00307837	Eef1a1	Elongation factor 1-alpha 1	Translation elongation factor activity, GTPase activity	137	0.67	Cytoplasm	0.0858
IPI00749677	Dnm2	Dynamin 2	GTPase activity	2	0.77	Cytoplasm	0.0313
IPI00317740	Gnb2l1	Guanine nucleotide-binding protein subunit	Protein kinase C binding	10	0.58	Cell membrane	0.1025

		beta-2-like 1, Rack1					
IPI0012938 3	Mettl1	tRNA (guanine-N(7)-)-methyltransferase	Methyl transferase activity	1	0.80	Nucleus	0.0052
IPI0045858 3	Hnrnpu	Heterogeneous nuclear ribonucleoprotein U	The formation of the inactive X chromosome (Xi), chromosome/RNA-binding	57	0.58	Nucleus	0.0614
IPI0064831 3	Srrm1	Serine/arginine repetitive matrix 1 isoform 2	DNA and RNA binding	8	1.4	Nucleus	0.0193
IPI0039995 3	Wnk1	Serine/threonine-protein kinase WNK1	Kinase activity	1	0.80	Cytoplasm	0.0105
IPI0055506 9	Pgk1	Phosphoglycerate kinase 1	Kinase activity	25	0.79	Cytoplasm	0.0157
IPI0042083 2	Mobkl3	Mps one binder kinase activator-like 3	Protein binding	2	1.64	Cytoplasm	0.2219
Ubiquitin proteasome							
IPI0033116 3	Skp1a	S-phase kinase-associated protein 1A	Ubiquitin-protein ligase activity	7	0.67	Cytoplasm	0.1177
IPI0031212 8	Trim28	Tripartite motif-containing 28, Transcription intermediary factor 1-beta (Tif1b)	Ubiquitin-protein ligase activity	39	0.51	Nucleoplasm	0.0859
IPI0041075 6	Arxes2	2900062L11Rik, adipocyte-related X-chromosome expressed sequence 2, Spcs3	Peptidase activity	1	0.55	Microsomes	0.1923
IPI0040365 0	Prss2	Anionic trypsin-2	Peptidase activity	26	1.65	Extracellular space	0.2750
Protein metabolism							
IPI0046606 9	Eef2	Elongation factor 2	Nucleotidyl transferase activity	82	0.46	Cytoplasm	0.0769
Oxidative stress							
IPI0075136 9	Ldha	L-lactate dehydrogenase	L-lactate dehydrogenase activity	31	0.62	Cytoplasm	0.0992
IPI0032359 2	Mdh2	Malate dehydrogenase	Oxidoreductase activity	34	0.61	Mitochondrial inner membrane	0.1447
Calcium ion binding protein							
IPI0012363 9	Calr	Calreticulin	Calcium ion binding	30	0.40	Endoplasmic reticulum lumen	0.0162
IPI0023054 0	Vdac1	Voltage-dependent anion-selective channel protein 1	Voltage-gated ion channel activity	28	0.78	Plasma membrane	0.0316
RNA helicase and RNA splicing factor activity							
IPI0011867 6	Eif4a1	Eukaryotic initiation factor 4A-I	RNA helicase activity	37	0.69	Cytoplasm	0.1043
Respiratory chain							
IPI0013028 0	Atp5a1	ATP synthase subunit alpha	Hydrolase activity	62	0.72	Mitochondrion inner membrane	0.0291

IPI00116074	Aco2	Aconitate hydratase	Hydro-lyase activity	32	0.58	Mitochondrion	0.1159
IPI00221398	Aldh18a1	Gamma-glutamyl phosphate reductase	Oxidoreductase activity	14	0.66	Mitochondrion inner membrane	0.0748
IPI00469268	Cct8	T-complex protein 1 subunit theta	ATP binding	49	0.64	Mitochondrion	0.0260
IPI00124073	Nxn	Nucleoredoxin	Oxidoreductase activity	2	3.56	Cytoplasm	1.6465
Cytoskeletal protein binding							
IPI00378015	Dbnl	Drebrin-like protein	Structural constituent of cytoskeleton	6	1.64	Cytoplasm	0.0924
IPI00227299	Vim	Vimentin	Structural constituent of cytoskeleton	52	0.73	Cytoplasm	0.0144
Amino acid transporter							
IPI00230351	Sdha	Succinate dehydrogenase [ubiquinone] flavoprotein subunit	Oxidoreductase activity	6	0.21	Mitochondrion inner membrane	0.3775
IPI00135977	Clic4	Chloride intracellular channel protein 4	Oxidoreductase activity	8	1.47	Cytoplasm	0.1259
IPI00131606	Tmem165	Transmembrane protein 165	-	2	1.6	Cytoplasmic vesicle membrane	0.1406
Protein metabolic process							
IPI00339916	Epr	Prolyl-tRNA synthetase	Aminoacyl-tRNA ligase activity	32	0.67	Cytoplasm	0.0556
IPI00469317	Sars	Seryl-tRNA synthetase	Aminoacyl-tRNA ligase activity	30	0.55	Cytoplasm	0.1658
IPI00230108	Pdia3	Protein disulfide-isomerase A3	Protein disulfide isomerase activity	50	0.63	Endoplasmic reticulum lumen	0.0210
IPI00311236	Rpl7	60S ribosomal protein L7	Structural constituent of ribosome	18	0.79	Cytosolic large ribosomal subunit	0.0104
IPI00133522	P4hb	Protein disulfide-isomerase	Protein disulfide isomerase activity	22	0.47	Endoplasmic reticulum lumen	0.1374
IPI00108143	Hnrnph2	Heterogeneous nuclear ribonucleoprotein H2	Structural constituent of ribosome	8	0.41	Nucleus	0.2617
IPI00124959	Mki67	Ki 67 protein, antigen identified by monoclonal antibody Ki 67	Cell proliferation	13	1.54	Nucleus	0.1493
IPI00111211	Mrpl46	39S ribosomal protein L46	Structural constituent of ribosome	1	0.75	Ribosome	0.0459
Other proteins							
IPI00132128	Rpa3	Replication protein A 14 kDa subunit	DNA repair	1	1.29	Nucleus	0.0331
IPI00230612	Gart	Phosphoribosylglycinamide formyltransferase	Transferase activity	10	0.69	Cytoplasm	0.0377
IPI001222	Top2a	DNA topoisomerase 2-	DNA	46	0.58	Nucleus	0.1170

23		alpha	topoisomerase activity				
IPI00132901	Lsm7	U6 snRNA-associated Sm-like protein LSm7	RNA splicing factor activity	1	1.90	Nucleus	0.3439
IPI00404707	Rbm14	RNA-binding protein 14	RNA splicing factor activity	6	0.61	Nucleus	0.1341
IPI00153400	H2afj	Histone H2A.J	DNA binding	57	1.21	Nucleus	0.0078
IPI00317794	Ncl	Nucleolin	RNA splicing factor activity	67	0.52	Nucleus	0.0515
IPI00187407	Cops8	COP9 signalosome complex subunit 8	Receptor binding	4	0.65	Cytoplasm	0.0784
IPI00117910	Prdx2	Peroxiredoxin-2	Oxidoreductase activity	16	0.77	Cytoplasm	0.0421
IPI00466621	Nol4	Nucleolar protein 4	unknown	1	1.43	Nucleolus	0.0366
Unclassified proteins							
IPI00282848	H3c1	Histone cluster 2, H3c1 isoform 2	DNA binding	16	2.63	Nucleus	0.9191
IPI00330679	Ddrgk1	DDRGK domain-containing protein 1	-	2	1.97	Endoplasmic reticulum	0.3852
IPI00903356	Cstf2	Cstf2 BetaCstF-64 variant 3	Nucleic acid binding	5	1.31	Nucleus	0.0820
IPI00131674	2210010C04Rik	Trypsinogen 7	Serine-type endopeptidase activity	4	1.41	-	0.1294
IPI00750004	EG668902	Similar to guanylate binding protein 5a	-	1	1.21	-	0.0078
IPI00679159	EG668144	Similar to ribosomal protein S3a	-	9	0.64	-	0.1240
IPI00462072	LOC100044223	Eno1;EG103324;EG433182 Alpha-enolase		90	0.57	-	0.1637
IPI00853739	Gm4492	100043516 similar to gag	-	66	0.80	Cytoplasm	0.0212
IPI00849828	Rpl30-ps7	100040182 similar to ribosomal protein L30, Gm2648	-	1	0.68	-	0.0718
IPI00625588	Gm9755	Hypothetical protein	-	4	0.76	-	0.0360
IPI00663587	Rbmxrt	RNA binding motif protein		7	0.66	Nucleus	0.0594
IPI00624840	-	12 kDa protein	-	64	0.48	Intermediate filament	0.1256
IPI00132575	Cotl1	Coactosin-like protein		2	0.36	Cytoplasm	0.3025
IPI00874996	-	23 kDa protein	-	17	0.31	Endoplasmic reticulum lumen	0.1509
IPI00124828	Mrps31	28S ribosomal protein S31	-	3	1.51	Mitochondria	0.1551

The list contains quantitative information of the proteins from tianma-stimulated differentiated mouse neuronal N2a cells compared with control. These proteins have met the criteria (i.e., unused ProtScore >2.0, 0.33 % (<1.0 %) FDR, change in expression levels of at least 1.2-fold (up-regulation) or at least <0.833-fold (down-regulation) as defined in the experimental procedures.

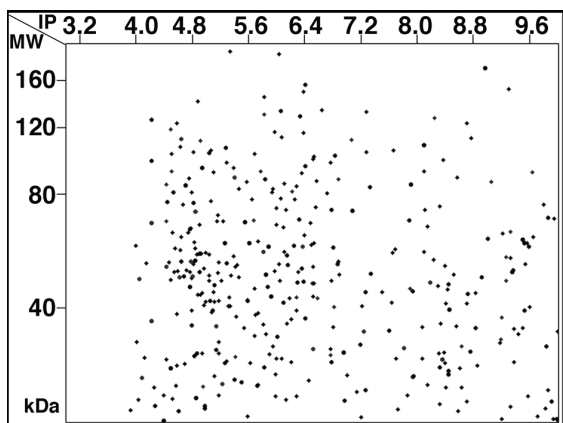*The total number of peptides identified with >95% confidence; C = control cells, T = tianma-treated cells.

Figure 3. Simulated 2D gel presentation of tianma-stimulated differentiated mouse neuronal N2a cells-derived quantified proteins. The proteins identified by LC-MS/MS were uploaded onto JvirGel, an online software used to create a 2D gel image. This image confirmed that the tissue-derived cell lysis performed was adequate and the entire proteome within cells was extracted. Isoelectric point (IP) and molecular weight (MW) values were generated from JVirGel at (http://www.jvirgel.de/).

Hspa5), with the cut-off for up- and down-regulation pre-defined at 1.2 and 0.83 respectively.

Classification of proteins regulated by tianma in differentiated N2a cells

We proceeded to use online databases (Panther, UniProt, and NCBI) to identify the func-

tions of these 74 proteins. During the classification process, our objective was also to identify the proteins' sub-cellular localization and activity (**Figure 4** and **Table 1**). It is of interest to note that a larger part of the identified affected proteins possess a DNA-binding activity (~46 %, **Figure 4A**) and are localized to the nucleus (~25 %, **Figure 4C**) though these nuclear proteins may contribute to various sub-cellular processes (e.g. chaperones, such as Hsp90, shuttle between cytoplasm and nucleus) as indicated by their equal 'process'-distributions (**Figure 4B**) as also shown by the reasonable distribution of their sub-cellular components (**Figure 4C**).

Proteins with possible neuro-protective roles and/or neuro-differentiation potential (e.g. Nxn, Dbnl, Mobkl3, Clic4, Mki67 and Bax), that are equally important for neuronal survival and synaptic plasticity during neuro-regenerative processes in the brain, were up-regulated upon tianma stimulation, while Sept2, Dnm2 and several stress-related proteins that can act as chaperones (Calr, Canx, Hsp70/90, Skp1a, Rack1 and Pdia3) were down-regulated (**Figure 4** and **Table 1**). Notably, a relatively high per centum of mitochondria (mt) (12 %), endoplasmic reticulum (ER)-resident (7 %) and "other membranes"-localized (e.g. ER or mt) = 7 %) proteins belonged to the altered proteins (**Figure 4C**). Many of the other proteins are actually part of multi-protein complexes or are involved in various metabolic functions, suggesting that tianma triggers the regulation of a diverse array of signalling pathways.
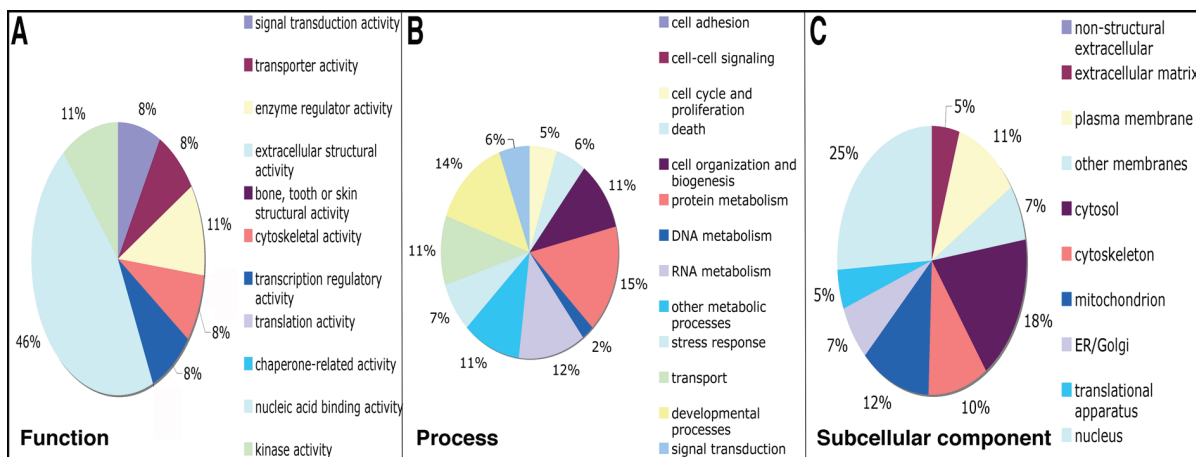

Figure 4. Pie chart depicting the identified proteins characterized by iTRAQ within the molecular function gene ontology (GO) category. Subcellular and functional processing categories (A-C) were based on the annotations of GO using the mouse genome informatics (MGI) GO_Slim Chart Tool. Representations of proteins based on the whole proteome quantified by iTRAQ.
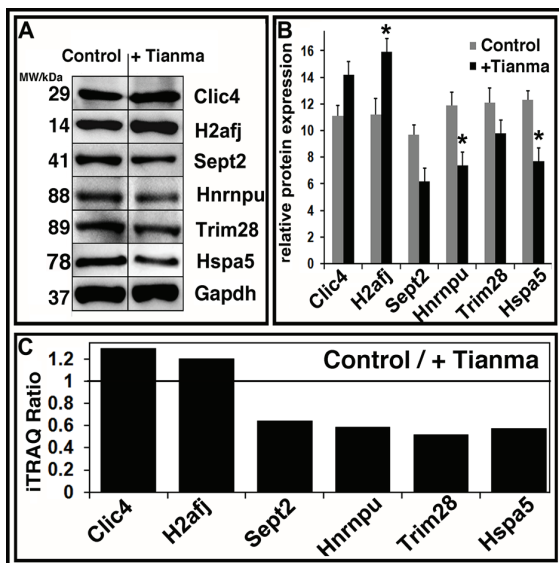
Figure 5. Western blot validation of iTRAQ results using protein samples from experimental batch I. (A) Randomly selected proteins regulated in tianma-activated differentiated neuronal N2a cells compared with controls. Clic4 and H2afj protein levels were increased and Sept2, Hnrnpu, Trim28 and Hspa5 levels were all reduced while Gapdh was unchanged. The western blots correlated with the iTRAQ values obtained. Gapdh was used as internal control. (B) Quantitative analyses of the western blots shown in A. Western blot experiments were performed at least three times for statistical quantification and analyses (n=3). Values (= relative protein expression) represent the ratio of densitometric scores for the respective western blot products and statistical error was indicated as mean ± SD (*$P < 0.05$, compared with controls) using the Gapdh bands as reference. (C) The histogram indicates a similar close relationship between iTRAQ and western blot expression ratios. Tianma-stimulated and control differentiated neuronal N2a cell iTRAQ expression ratios from selected proteins were consistent with the western blot results and thus validated a strong agreement in the expression data.

Figure 6. Western blot validation of iTRAQ results using protein samples from experimental batch II. (A) Randomly selected proteins regulated in tianma-activated differentiated neuronal N2a cells compared with controls. Vim, Calr, Hsp90 and Sept2 levels were all reduced while Gapdh was unchanged. The western blots correlated with the iTRAQ values obtained. Gapdh was used as internal control. (B) Quantitative analyses of the western blots shown in A. Western blot experiments were performed at least three times for statistical quantification and analyses (n=3). Values (= relative protein expression) represent the ratio of densitometric scores for the respective western blot products and statistical error was indicated as mean ± SD (*$P < 0.05$, compared with controls) using the Gapdh bands as reference. (C) The histogram indicates a similar close relationship between iTRAQ and western blot expression ratios. Tianma-stimulated and control differentiated neuronal N2a cell iTRAQ expression ratios from selected proteins were consistent with the western blot results and thus validated a strong agreement in the expression data.

Validation of tianma-regulated proteins

Following the database search and classification of proteins, western blots were performed on randomly selected proteins to verify the iTRAQ values. Seven randomly selected proteins from batch-I (**Figure 5**) (Clic4, H2afj, Sept2, Hnrnpu, Trim28, Hspa5 and Gapdh) and five randomly selected proteins from batch-II (Vim, Calr, Hsp90, Sept2 and Gapdh) were used for iTRAQ data validation (**Figure 6**). Gapdh was used as an internal control to ensure equal
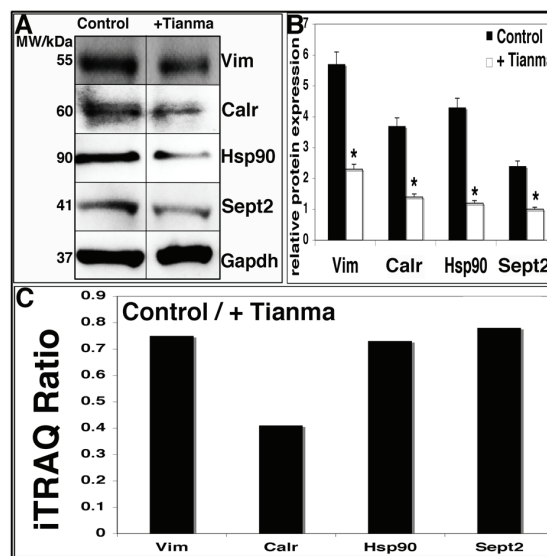
loading of samples as its level was unchanged in the iTRAQ analysis.

Notably, the western blot images correlated very well and thus confirmed the iTRAQ values obtained.

STRING protein–protein interaction analysis of tianma-modulated proteins

STRING (Search Tool for the Retrieval of Interacting Genes) is a database resource dedicated to protein–protein interactions, including both

physical and functional interactions. It weighs and integrates information from numerous sources, including experimental repositories, computational prediction methods and public text collections, thus acting as a meta-database that maps all interaction evidence onto a common set of genomes and proteins [23]. This analysis provides an essential neural systems-level understanding of cellular events in a functional neuron. Functional partnerships between proteins are at the core of complex cellular phenotypes, and the networks formed by interacting proteins provided us with crucial scaffolds for modeling and data reduction to get insight into the mechanisms involved in tianma-affected neural functions. For our current study it reveals the functional link among chaperone proteins such as Canx, Calr, Pdia3, Hsp70, Hsp90, Skp1a, Trim28, Gnb2l1 (Rack1), Bax, and their potential link to other metabolically modulated proteins such as Hnrnpu, Prss2, Mdh2, Atp5a1, Vdac1, Vim or Prdx2 (**Figure 7**).

IPA signalling pathway analysis of tianma-modulated proteins

Further bio-computational network analysis of the proteins identified in tianma-stimulated differentiated N2a neurons using the Ingenuity Pathways Analysis (IPA) offered us additional valuable clues about the complex interactive link of the various identified proteins within their commonly known interactive protein networks also obtained from other cellular metabolic information (**Figure 8**).

In addition, neural-specific IPA analysis could demonstrate the involvement of the iTRAQ-based analysis-identified proteins and their metabolic interactive pathways within a neuronal network, eventually important for the proper functions of active neurons in the central nervous system (CNS) during neuro-regenerative processes such as neural plasticity.

In particular it could demonstrate the network among proteins from various intracellular localizations with important roles in cell survival and differentiation that were previously considered as difficult to detect [24, 25], such as the nucleus (e.g. Nol4, Cnbp or Hnf4a), mt (e.g. Mrpl46 or Mrp231), and the cytoplasm (Eif4a1) as well as several other metabolic (Mdm2, Cdk5, Cdkn1b) and survival-controlling (Gfer

(linked to the Cop9-signalosome protein complex (Cops7/8) [26]), Pdcd4 and Bax) enzymes (**Figure 9**).

Discussion

Orchids and their derivatives have been used for many years in clinical studies to treat various neuronal disorders and demonstrated a powerful effect [4, 6]. In our previous study, we could demonstrate the effect of tianma on cognitive functions in mice [12]. Here, we provide an additional interesting insight into the molecular and cellular mechanisms of herbal medicine by disclosing the effect of tianma on the full neuronal proteome changes upon stimulation of differentiated mouse neuronal N2a cells. In the following sections we briefly discuss the identified proteins that were found to be altered upon neuronal tianma stimulation and we hypothesize potential applications of tianma that may emerge from our data obtained:

Increased neuro-protective protein levels in differentiated neuronal N2a cells upon tianma activation

Nxn: Nucleoredoxin is a novel thioredoxin family member that is involved in cell growth and differentiation where it sustains Wnt/β-catenin signalling by retaining a pool of inactive dishevelled protein [27-29]. Its activation by tianma allows the herb to influence pivotal neuronal differentiation pathways. In fact, we observed slightly enhanced neurite extension formation after adding tianma to the neuronal cells (**Figure 2C**).

Dbnl: Similarly, tianma partakes in cell differentiation processes by mobilizing Dbnl [30]. Dbnl deficiency leads to tissue and behavioral abnormalities and impaired vesicle transport [31]. It is a cytoskeletal protein that may serve as a signal-responsive link between the dynamic cortical actin cytoskeleton and regions of membrane dynamics such as neurite-outgrowth processes and synaptic plasticity [32].

Mobkl3: Mobkl3 is both a member and a putative substrate of striatin family-protein phosphatase 2A (PP2A) complexes [33], an enzyme that belongs to a highly regulated family of serine/threonine phosphatases implicated in cell growth and signalling [34] which has been shown to participate in various signalling events
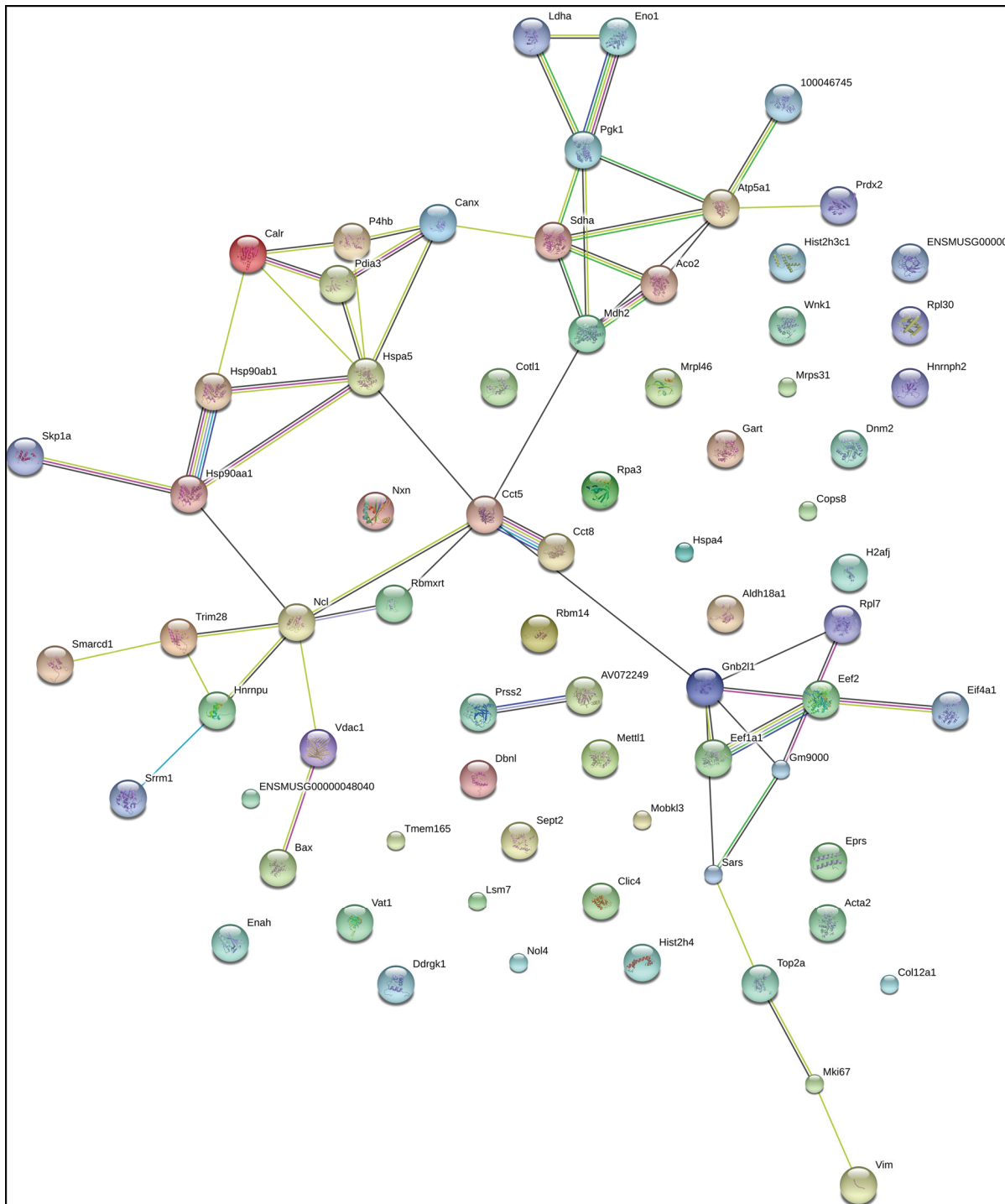
Figure 7. STRING-9.0 analysis (*mus musculus* at: (http://string-db.org/); parameters: default setting) of tianma-modulated proteins in differentiated neuronal N2a cells: Different line colors represent the types of evidence for the association. Network display: Nodes are either colored (if they are directly linked to the input as in the table 1) or white (nodes of a higher iteration). Edges, i.e. predicted functional links, consist of up to eight lines: one color for each type of evidence.

crucially involved in neurodegenerative processes [35, 36]. This adds a further interesting

aspect on tianma's potential application for a possible treatment of neurological diseases [4,
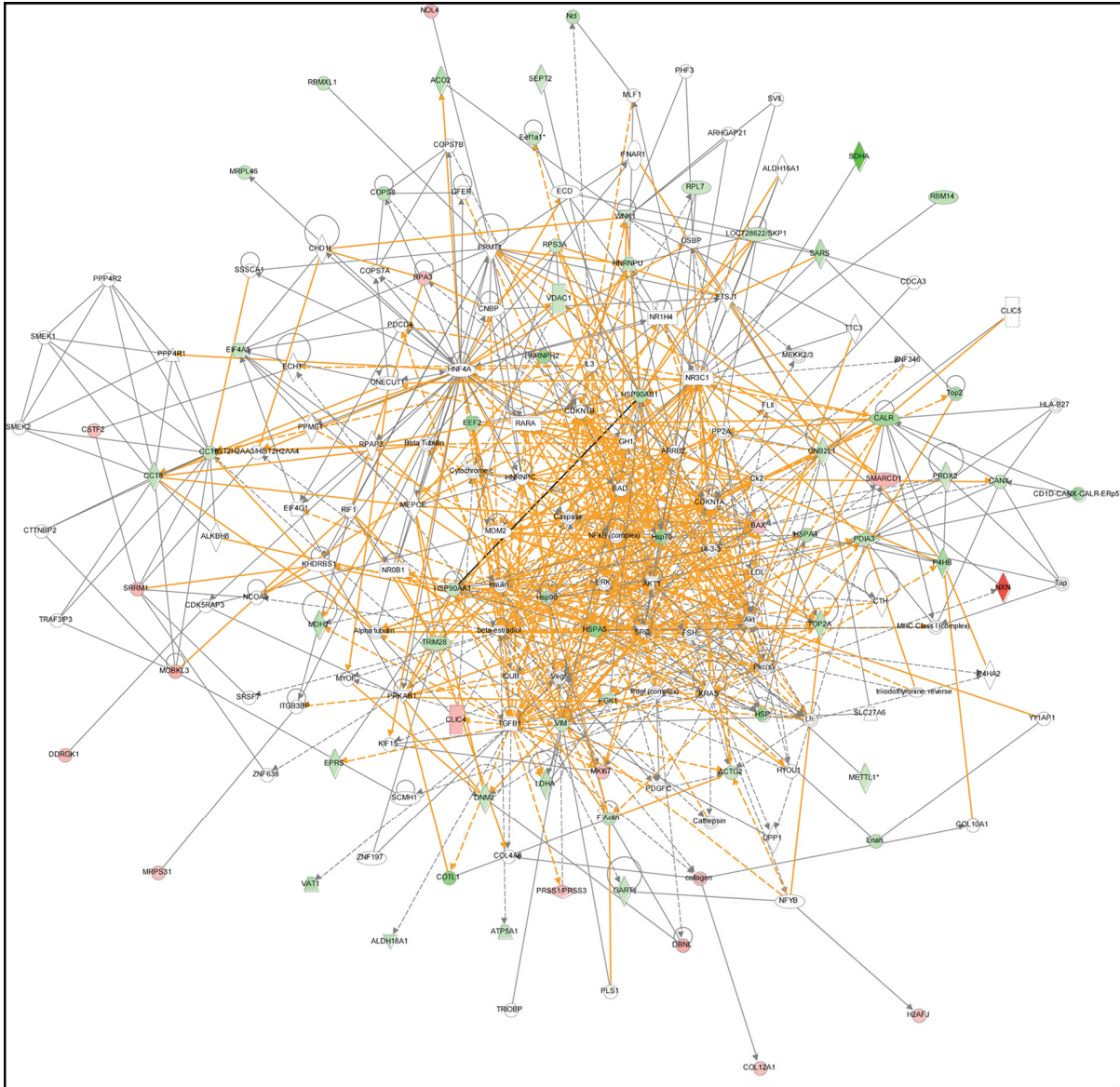
Figure 8. Network analysis of proteins identified in tianma-stimulated differentiated neuronal N2a cells using the IPA. Five IPA-provided major networks were merged and analyzed based on the iTRAQ data of proteins expressed in tianma-activated differentiated neuronal N2a cells. Network-1: included protein activities (e.g. the iTRAQ analysis-identified proteins: BAX, CALR, CANX, DBNL, HSP90AA1, HSPA4, HSPA5, PRDX2 and others) related to post-translational modification, protein folding, cellular function and maintenance; Network-2: included protein activities (e.g. the iTRAQ analysis-identified proteins: RBM14, RPA3, WNK1, SEPT2, HNRNPH2 and others) related to amino acid metabolism, small molecule biochemistry, cellular growth and proliferation; Network-3: included protein activities (e.g. the iTRAQ analysis-identified proteins: COL12A1, ATP5A1, SRRM1, VAT1, NXN and others) related to drug metabolism, lipid metabolism, and small molecule biochemistry; Network-4: included protein activities (e.g. the iTRAQ analysis-identified proteins: TRIM28, VIM, MDH2 DBNL, DNM2, GNB2L1, PRSS1/3 and others) related to general cancer and genetic disorders; Network-5: included protein activities (e.g. the iTRAQ analysis-identified proteins: COPS8, MRPL46, MRPS31, NOL4, and others) related to cell cycle, cellular development, nervous system, development and function. The solid lines refer to a direct protein-protein interaction, while dotted lines show an indirect relationship among the iTRAQ-based identified genes.

12].

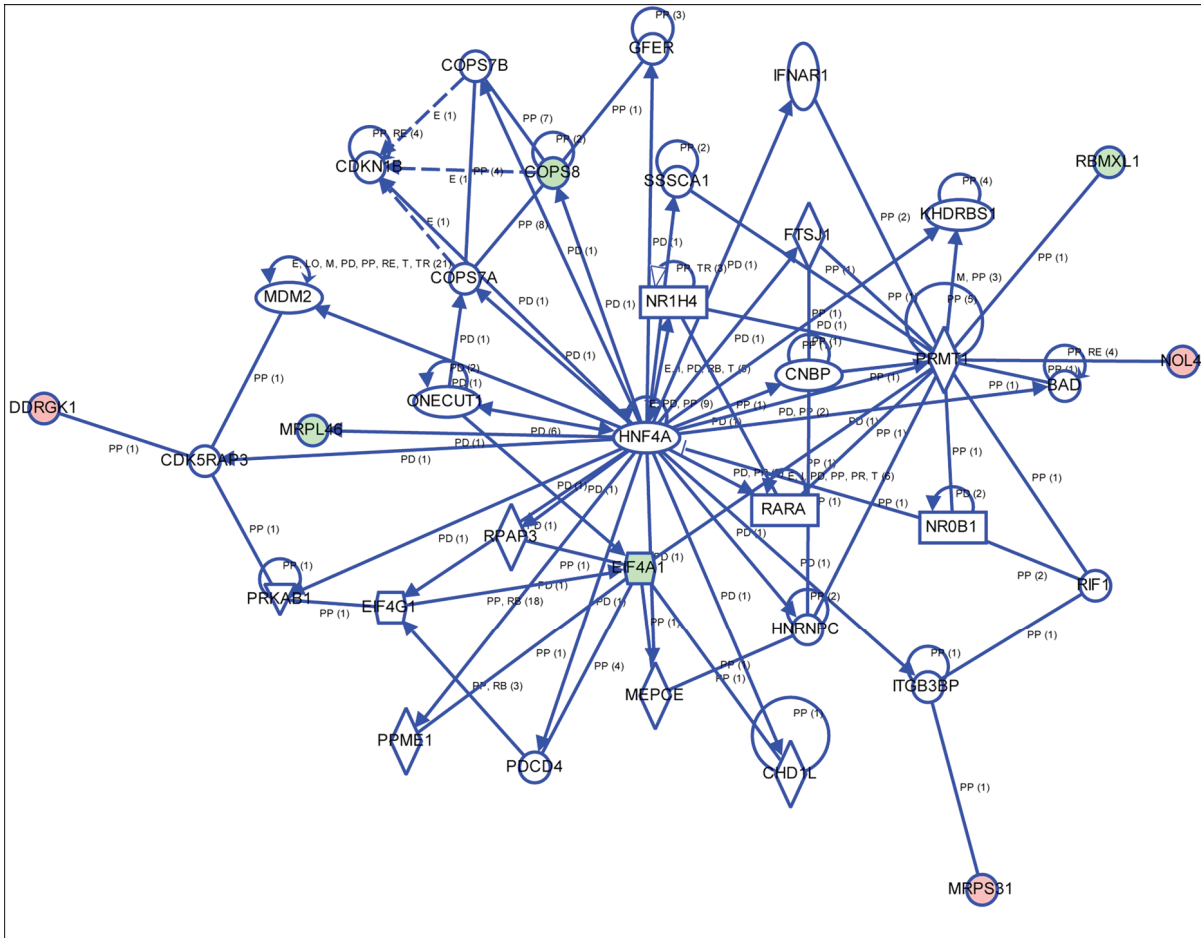*Clic4*: Clic4 (chloride intracellular channel 4) is a multifunctional protein that localizes to the mt

Figure 9. Neuronal-specific network analysis of iTRAQ-based proteomic metabolism in tianma-activated differentiated mouse neuronal N2a cells using IPA. IPA analysis for the understanding how the identified proteins work together by protein-protein interactions within the context of nervous-system-related metabolic signalling pathways that affect cellular changes in the nervous system induced by neural tianma stimulation.

and cytoplasm and also traffics between the cytoplasm and nucleus while it interacts with Schnurri-2, a transcription factor in the bone morphogenetic protein (BMP) signalling pathway. Transforming growth factor beta (TGF-beta) promotes the expression of Clic4 and Schnurri-2 as well as their association in the cytoplasm and their translocation to the nucleus. In the absence of Clic4 or Schnurri-2, TGF-beta signalling is abrogated. Direct nuclear targeting of Clic4 enhances TGF-beta signalling and removes the requirement for Schnurri-2. Nuclear Clic4 associates with phospho (p)-Smad2 and p-Smad3, protecting them from dephosphorylation by nuclear phosphatases. These result in newly identified Clic4 as modifier of TGF-beta signalling through its function as stabilizer of p-

Smad2 and 3 in the nucleus which is essential for Clic4-mediated growth-arrest and differentiation [37]. In addition, Clic4 mediates TGF-beta1-induced fibroblast-to-myofibroblast trans-differentiation [38] and is required for Ca2+-induced keratinocyte differentiation [39]. Proteomic analysis of vascular endothelial growth factor-induced endothelial cell differentiation reveals a role for Clic4 in tubular morphogenesis also hinting at its involvement in neuronal differentiation processes [40]. Furthermore, Clic4 could be involved in mt-membrane potential generation in mtDNA-depleted cells, a feature required to prevent apoptosis and to drive continuous protein import into mt [41]. Besides, in response to cellular stress Clic4 translocates to the nucleus for the control of apoptotic proc-
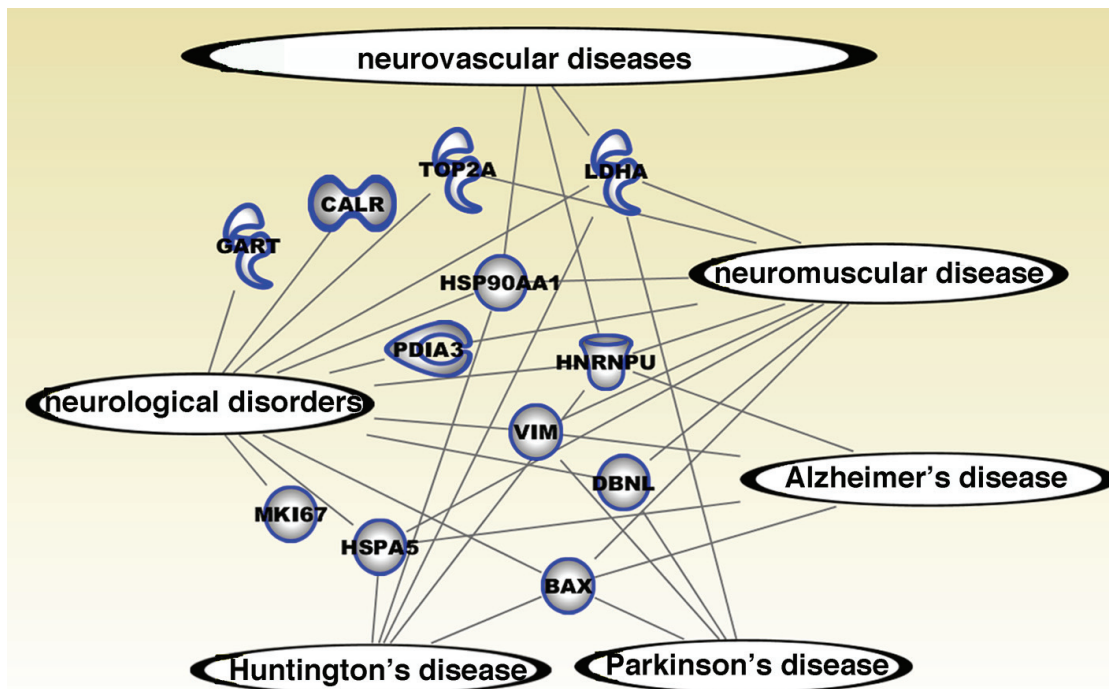
Figure 10. Neurodegenerative-diseases-specific network analysis of iTRAQ-based proteomic metabolism in tianma-activated differentiated mouse neuronal N2a cells using IPA. IPA analysis deciphered a group of identified proteins modulated by neural tianma stimulation and their potential interactive link within the context of various neurodegenerative-diseases.

esses [42] making it another pivotal protein of the tianma-activated signalling cascade.

Mki67: The up-regulation of Mki67 (though rather considered as a proliferative marker) has also been observed previously for *ginkgo biloba* during the stimulation of neurogenesis [43]. The significance of this finding, however, still needs further detailed investigations.

Bax: Bax is a nuclear-encoded protein present in higher eukaryotes that is able to pierce the mt-outer membrane to mediate cell death by apoptosis [44]. However, a recent report demonstrated a non-apoptotic function of Bax in long-term depression of synaptic transmission with caspase-3 activation and Bax modulation as pivotal elements during synaptic plasticity [45]. Thus, fine tuning of bax and caspase-3 may contribute to tianma-mediated synaptic plasticity as part of tianma's effect on cognitive functions [12].

Decreased levels of GTPases and stress-related proteins in differentiated neuronal N2a cells upon tianma stimulation

Sept2: Septins are an evolutionarily conserved group of GTP-binding and filament-forming proteins that belong to the large superclass of P-loop GTPases. Their expression is tightly regulated to maintain proper filament assembly and normal cellular functions. Septins perform diverse cellular functions according to tissue expression and their interacting partners. Functions identified to date include cell apoptosis, DNA damage response and alterations of these septin scaffolds, by mutation or expression changes, have been associated with a variety of neurological diseases such as AD and Parkinson's disease (PD) [46, 47]. As other Rho GTPases [48, 49], Sept2 is crucially involved in modeling neurite outgrowth during neuronal differentiation and a tight regulation of its expression is necessary [50].

Dnm2: Dynamin 2 (Dnm2) is a large GTPase mainly involved in membrane trafficking through its function in the formation and release of nascent vesicles from biological membranes. Additionally, it tightly interacts with and is involved in the regulation of actin and microtubule networks, independent from membrane trafficking

processes. Functional data on Dnm2 reveals the possible pathophysiological mechanisms via which Dnm2 mutations can lead to two distinct neuromuscular disorders. Dnm2 mutations cause autosomal dominant centronuclear myopathy, a rare form of congenital myopathy, and intermediate and axonal forms of Charcot–Marie-Tooth disease, a peripheral neuropathy [51, 52]. Furthermore, altered expression of Dnm2 has been observed in AD [53].

Wnk1: Wnk1 is a Ser/Thr protein kinase and mutations in the nervous system-specific HSN2 exon of Wnk1 cause hereditary sensory neuropathy type II [54]. Moreover, Wnk1 was identified to interact with Rho-GDI1 to regulate Lingo1 -mediated inhibition of neurite extension [55].

Prdx2: Peroxiredoxins are antioxidant enzymes involved in protein and lipid protection against oxidative injury and in cellular signalling pathways regulating apoptosis. In the CNS, Prdx2 has been shown to be expressed in neurons and its de-regulation has been associated with several neurodegenerative diseases such as AD and PD [56-59].

Tianma modulates (ER-resident) molecular chaperone proteins in differentiated neuronal N2a cells

Skp1a: Decreased expressions of the ubiquitin-proteasome/E3 ligase component Skp1a and the chaperone Hsc-70 can lead to a wide impairment in the function of an entire repertoire of proteins in neurons [60] suggesting a new structural role of Skp1a in dopaminergic neuronal functions besides its E3 ligase activity [61]. The close relation between apoptotic and neuronal differentiation pathways raises the question about the significance of tianma-mediated inhibition of Skp1a protein expression in differentiated neuronal N2a cells [62, 63].

Hsp90aa1, Hsp90ab1, Hspa4, Hspa5: The heat shock protein (HSP) family has long been associated with a generalized cellular stress response, particularly in terms of recognizing and chaperoning misfolded proteins. HSPs are induced in response to many injuries including stroke, neurodegenerative diseases, epilepsy, and trauma. Hsp70 has a multifaceted role in neurons. It serves a protective role in several different models of nervous system injury. For instance, Hsp70 functions as a chaperone and protects neurons from protein aggregation and toxicity (in PD, AD, polyglutamine diseases, and amyotrophic lateral sclerosis), protects cells from apoptosis (PD), is a stress marker (temporal lobe epilepsy), and also protects cells from cerebral ischemic injury. However, it has also been linked to a deleterious role in some diseases [64, 65]. In particular, it has been shown very recently that Hsp70 can suppress AD phenotypes in mice [66]. The main function of Hsp90 complexes is to maintain protein quality control and to assist in protein degradation via proteasomal and autophagic-lysosomal pathways. As such it plays a major role in the pathology of AD where it is crucially involved (with co-chaperones such as the immunophilins FKBP51 and FKBP52) in the control of aberrant phosphorylated tau protein [67]. Thus, alongside Mobkl3 and PP2A, tianma can eventually influence aberrant tau phosphorylation by modulating Hsp90 action [35, 36, 68].

Canx: Calnexin is an ER-resident molecular chaperone that plays an essential role in the correct folding of membrane proteins and a component of the quality control of the secretory pathway. Canx gene-deficient mice showed that Canx deficiency leads to myelinopathy [69]. In addition, Canx (-/-) cells have an increased constitutively active unfolded protein response (UPR). Importantly, Canx (-/-) cells have significantly increased proteasomal activity, which may play a role in the adaptive mechanisms addressing the acute ER stress observed in the absence of Canx [70]. Besides, caspase-3 or caspase-7 cleaves Canx, whose cleaved product, very interestingly, leads to the attenuation of apoptosis [71].

Trim28: In neurons disruption of Trim28, a key component of transcriptional repressor complexes in the brain, results in increased anxiety-like behavior and sensitivity to stress [72].

Calr: Calreticulin is a soluble calcium-binding chaperone of the ER that is also detected on the cell surface and in the cytosol. The protein is involved in the regulation of intracellular Ca^{2+} homeostasis and ER Ca^{2+} storage capacity. Calr is also an important molecular chaperone involved in quality control within secretory pathways. As such, it is involved in the folding of newly synthesized proteins and glycoproteins and, together with calnexin (an integral ER membrane chaperone similar to Calr) and Pdia3 (ERp57, an ER protein of 57 kDa; a PDI (protein disulfide-isomerase)-like ER-resident protein), it

constitutes the 'calreticulin/calnexin cycle' that is responsible for folding and quality control of newly synthesized glycoproteins. In fact, during recent years, Calr has been implicated to play a pivotal role in many biological systems, including functions inside and outside the ER, indicating that the protein is a multi-process molecule [73-75] that might be involved as an ER-resident chaperone in AD and PD [76-78].

Pdia3: Pdia3 is an ER-resident thiol-disulfide oxidoreductase which is modulating Stat3 (signal transducer and activator of transcription) signalling from the lumen of the ER together with Calr [79, 80] that might be affected by PD [81].

Gnb2l1: This guanine nucleotide binding protein (G protein), also known as Rack1 (receptor for activated protein kinase C 1), regulates intracellular Ca^{2+} levels, potentially contributing to processes such as learning, memory and synaptic plasticity by binding specifically to an ionotropic glutamate receptor and thereby dictating neuronal excitation and sensitivity [82].

Atp5a1: Mt-ATP synthase catalyzes ATP synthesis, utilizing an electrochemical gradient of protons across the inner membrane during oxidative phosphorylation. It seems obvious that even intermittent and minor impairment of this highly important enzyme could deprive the brain tissue of energy at crucial times, which may predispose or contribute to neurological diseases [83].

Concluding, our data has shed new insights on the possible involvement of the herb tianma on neuronal functions and its potential effect on signalling molecules critically involved in common neurorestorative processes related to neurodegenerative diseases such as AD, PD or Huntington's disease (**Figure 10**). However, further systemic functional *in/ex vivo* biology studies are required to decipher the functional significance of the individual bioactive components of tianma, by phytochemistry, to unravel their direct effect on neuronal activities related to neuroprotective activities in order to open new potential avenues based on tianma for the possible treatment of neurodegenerative diseases such as AD [4, 84, 85].

Acknowledgement

Abbreviations: iTRAQ, isobaric tags for relative and absolute quantitation.

Address correspondence to: Dr. Klaus Heese, Institute of Advanced Studies, Nanyang Technological University, 60 Nanyang View, Singapore 639673, Singapore. Tel: +65-6316-2848; Fax: +65-6791-3856; E-mail: klaus.heese@rub.de

References

[1]   Schachter SC. Botanicals and herbs: a traditional approach to treating epilepsy. Neurotherapeutics 2009; 6: 415-420.

[2]   Sucher NJ. Insights from molecular investigations of traditional Chinese herbal stroke medicines: implications for neuroprotective epilepsy therapy. Epilepsy Behav 2006; 8: 350-362.

[3]   Yuan R and Lin Y. Traditional Chinese medicine: an approach to scientific proof and clinical validation. Pharmacol Ther 2000; 86: 191-198.

[4]   Hew CS and Yong JWH. Orchids in Chinese medicine. Innovation 2007; 6: 2-4.

[5]   Bulpitt CJ. The uses and misuses of orchids in medicine. QJM 2005; 98: 625-631.

[6]   Bulpitt CJ, Li Y, Bulpitt PF and Wang J. The use of orchids in Chinese medicine. J R Soc Med 2007; 100: 558-563.

[7]   Hsieh MT, Wu CR and Chen CF. Gastrodin and p -hydroxybenzyl alcohol facilitate memory consolidation and retrieval, but not acquisition, on the passive avoidance task in rats. J Ethnopharmacol 1997; 56: 45-54.

[8]   Kim HJ, Moon KD, Oh SY, Kim SP and Lee SR. Ether fraction of methanol extracts of Gastrodia elata, a traditional medicinal herb, protects against kainic acid-induced neuronal damage in the mouse hippocampus. Neurosci Lett 2001; 314: 65-68.

[9]   Kim HJ, Moon KD, Lee DS and Lee SH. Ethyl ether fraction of Gastrodia elata Blume protects amyloid beta peptide-induced cell death. J Ethnopharmacol 2003; 84: 95-98.

[10] Kim HJ, Lee SR and Moon KD. Ether fraction of methanol extracts of Gastrodia elata, medicinal herb protects against neuronal cell damage after transient global ischemia in gerbils. Phytother Res 2003; 17: 909-912.

[11] Ong ES, Heng MY, Tan SN, Hong Yong JW, Koh H, Teo CC and Hew CS. Determination of gastrodin and vanillyl alcohol in Gastrodia elata Blume by pressurized liquid extraction at room temperature. J Sep Sci 2007; 30: 2130-2137.

[12] Mishra M, Huang J, Lee YY, Chua DS, Lin X, Hu JM and Heese K. Gastrodia elata modulates amyloid precursor protein cleavage and cognitive functions in mice. Biosci Trends 2011; 5: 129-138.

[13] Datta A, Park JE, Li X, Zhang H, Ho ZS, Heese K,

Lim SK, Tam JP and Sze SK. Phenotyping of an in vitro model of ischemic penumbra by iTRAQ-based shotgun quantitative proteomics. J Proteome Res 2010; 9: 472-484.

[14] Datta A, Jingru Q, Khor TH, Teo MT, Heese K, and Sze SK. Quantitative Neuroproteomics of an in vivo rodent model of focal cerebral ischemia/reperfusion injury reveals a temporal regulation of novel pathophysiological molecular markers.. J Proteome Res 2011; 10: 5199-5213.

[15] Zhang GM and Yang LX. Research and development of Zhaotong tianma. In: editors. Yunnan Science and Techonology Press; 2007. p. 86-91.

[16] Li N, Wang KJ, Chen JJ and Zhou J. Phenolic compounds from the rhizomes of Gastrodia elata. J Asian Nat Prod Res 2007; 9: 373-377.

[17] Sundaramurthi H, Manavalan A, Ramachandran U, Hu JM, Sze SK and Heese K. Phenotyping of tianma-stimulated differentiated rat neuronal b104 cells by quantitative proteomics. Neurosignals 2012; 20: 48-60.

[18] Mishra M, Manavalan A, Sze SK and Heese K. Neuronal p60TRP expression modulates cardiac capacity. J Proteomics 2012; 75: 1600-1617.

[19] Islam O, Loo TX and Heese K. Brain-derived neurotrophic factor (BDNF) has proliferative effects on neural stem cells through the truncated TRK-B receptor, MAP kinase, AKT, and STAT-3 signaling pathways. Curr Neurovasc Res 2009; 6: 42-53.

[20] Shen Y, Inoue N and Heese K. Neurotrophin-4 (ntf4) mediates neurogenesis in mouse embryonic neural stem cells through the inhibition of the signal transducer and activator of transcription-3 (stat3) and the modulation of the activity of protein kinase B. Cell Mol Neurobiol 2010; 30: 909-916.

[21] Mishra M, Akatsu H and Heese K. The novel protein MANI modulates neurogenesis and neurite-cone growth. J Cell Mol Med 2011; 15: 1713-1725.

[22] Hiller K, Schobert M, Hundertmark C, Jahn D and Munch R. JVirGel: Calculation of virtual two-dimensional protein gels. Nucleic Acids Res 2003; 31: 3862-3865.

[23] Szklarczyk D, Franceschini A, Kuhn M, Simonovic M, Roth A, Minguez P, Doerks T, Stark M, Muller J, Bork P, Jensen LJ and von Mering C. The STRING database in 2011: functional interaction networks of proteins, globally integrated and scored. Nucleic Acids Res 2011; 39: D561-568.

[24] Ueki N, Oda T, Kondo M, Yano K, Noguchi T and Muramatsu M. Selection system for genes encoding nuclear-targeted proteins. Nat Biotechnol 1998; 16: 1338-1342.

[25] Pagliarini DJ, Calvo SE, Chang B, Sheth SA, Vafai SB, Ong SE, Walford GA, Sugiana C, Boneh A, Chen WK, Hill DE, Vidal M, Evans JG, Thorburn DR, Carr SA and Mootha VK. A mitochondrial protein compendium elucidates complex I disease biology. Cell 2008; 134: 112-123.

[26] Sankar U and Means AR. Gfer is a critical regulator of HSC proliferation. Cell Cycle 2011; 10: 2263-2268.

[27] Funato Y, Terabayashi T, Sakamoto R, Okuzaki D, Ichise H, Nojima H, Yoshida N and Miki H. Nucleoredoxin sustains Wnt/beta-catenin signaling by retaining a pool of inactive dishevelled protein. Curr Biol 2010; 20: 1945-1952.

[28] Funato Y and Miki H. Nucleoredoxin, a novel thioredoxin family member involved in cell growth and differentiation. Antioxid Redox Signal 2007; 9: 1035-1057.

[29] Funato Y, Michiue T, Asashima M and Miki H. The thioredoxin-related redox-regulating protein nucleoredoxin inhibits Wnt-beta-catenin signalling through dishevelled. Nat Cell Biol 2006; 8: 501-508.

[30] Cortesio CL, Perrin BJ, Bennin DA and Huttenlocher A. Actin-binding protein-1 interacts with WASp-interacting protein to regulate growth factor-induced dorsal ruffle formation. Mol Biol Cell 2010; 21: 186-197.

[31] Connert S, Wienand S, Thiel C, Krikunova M, Glyvuk N, Tsytsura Y, Hilfiker-Kleiner D, Bartsch JW, Klingauf J and Wienands J. SH3P7/mAbp1 deficiency leads to tissue and behavioral abnormalities and impaired vesicle transport. EMBO J 2006; 25: 1611-1622.

[32] Kessels MM, Engqvist-Goldstein AE and Drubin DG. Association of mouse actin-binding protein 1 (mAbp1/SH3P7), an Src kinase target, with dynamic regions of the cortical actin cytoskeleton in response to Rac1 activation. Mol Biol Cell 2000; 11: 393-412.

[33] Moreno CS, Lane WS and Pallas DC. A mammalian homolog of yeast MOB1 is both a member and a putative substrate of striatin family-protein phosphatase 2A complexes. J Biol Chem 2001; 276: 24253-24260.

[34] Janssens V and Goris J. Protein phosphatase 2A: a highly regulated family of serine/threonine phosphatases implicated in cell growth and signalling. Biochem J 2001; 353: 417-439.

[35] Tanimukai H, Kudo T, Tanaka T, Grundke-Iqbal I, Iqbal K and Takeda M. Novel therapeutic strategies for neurodegenerative disease. Psychogeriatrics 2009; 9: 103-109.

[36] Mishra M and Heese K. P60TRP interferes with the GPCR/secretase pathway to mediate neuronal survival and synaptogenesis. J Cell Mol Med 2011; 15: 2462-2477.

[37] Shukla A, Malik M, Cataisson C, Ho Y, Friesen T, Suh KS and Yuspa SH. TGF-beta signalling is regulated by Schnurri-2-dependent nuclear translocation of CLIC4 and consequent stabilization of phospho-Smad2 and 3. Nat Cell Biol 2009; 11: 777-784.

[38] Yao Q, Qu X, Yang Q, Wei M and Kong B. CLIC4 mediates TGF-beta1-induced fibroblast-to-myofibroblast transdifferentiation in ovarian cancer. Oncol Rep 2009; 22: 541-548.

[39] Suh KS, Mutoh M, Mutoh T, Li L, Ryscavage A, Crutchley JM, Dumont RA, Cheng C and Yuspa SH. CLIC4 mediates and is required for Ca2+-induced keratinocyte differentiation. J Cell Sci 2007; 120: 2631-2640.

[40] Bohman S, Matsumoto T, Suh K, Dimberg A, Jakobsson L, Yuspa S and Claesson-Welsh L. Proteomic analysis of vascular endothelial growth factor-induced endothelial cell differentiation reveals a role for chloride intracellular channel 4 (CLIC4) in tubular morphogenesis. J Biol Chem 2005; 280: 42397-42404.

[41] Arnould T, Mercy L, Houbion A, Vankoningsloo S, Renard P, Pascal T, Ninane N, Demazy C and Raes M. mtCLIC is up-regulated and maintains a mitochondrial membrane potential in mtDNA-depleted L929 cells. FASEB J 2003; 17: 2145-2147.

[42] Suh KS, Mutoh M, Nagashima K, Fernandez-Salas E, Edwards LE, Hayes DD, Crutchley JM, Marin KG, Dumont RA, Levy JM, Cheng C, Garfield S and Yuspa SH. The organellular chloride channel protein CLIC4/mtCLIC translocates to the nucleus in response to cellular stress and accelerates apoptosis. J Biol Chem 2004; 279: 4632-4641.

[43] Yoo DY, Nam Y, Kim W, Yoo KY, Park J, Lee CH, Choi JH, Yoon YS, Kim DW, Won MH and Hwang IK. Effects of Ginkgo biloba extract on promotion of neurogenesis in the hippocampal dentate gyrus in C57BL/6 mice. J Vet Med Sci 2011; 73: 71-76.

[44] Westphal D, Dewson G, Czabotar PE and Kluck RM. Molecular biology of Bax and Bak activation and action. Biochim Biophys Acta 2011; 1813: 521-531.

[45] Jiao S and Li Z. Nonapoptotic function of BAD and BAX in long-term depression of synaptic transmission. Neuron 2011; 70: 758-772.

[46] Peterson EA and Petty EM. Conquering the complex world of human septins: implications for health and disease. Clin Genet 2010; 77: 511-524.

[47] Hall PA and Russell SE. The pathobiology of the septin gene family. J Pathol 2004; 204: 489-505.

[48] Luo L. Rho GTPases in neuronal morphogenesis. Nat Rev Neurosci 2000; 1: 173-180.

[49] Hirose M, Ishizaki T, Watanabe N, Uehata M, Kranenburg O, Moolenaar WH, Matsumura F, Maekawa M, Bito H and Narumiya S. Molecular dissection of the Rho-associated protein kinase (p160ROCK)-regulated neurite remodeling in neuroblastoma N1E-115 cells. J Cell Biol 1998; 141: 1625-1636.

[50] Vega IE and Hsu SC. The septin protein Nedd5 associates with both the exocyst complex and microtubules and disruption of its GTPase activity promotes aberrant neurite sprouting in PC12 cells. Neuroreport 2003; 14: 31-37.

[51] Durieux AC, Prudhon B, Guicheney P and Bitoun M. Dynamin 2 and human diseases. J Mol Med (Berl) 2010; 88: 339-350.

[52] Fabrizi GM, Ferrarini M, Cavallaro T, Cabrini I, Cerini R, Bertolasi L and Rizzuto N. Two novel mutations in dynamin-2 cause axonal Charcot-Marie-Tooth disease. Neurology 2007; 69: 291-295.

[53] Kamagata E, Kudo T, Kimura R, Tanimukai H, Morihara T, Sadik MG, Kamino K and Takeda M. Decrease of dynamin 2 levels in late-onset Alzheimer's disease alters Abeta metabolism. Biochem Biophys Res Commun 2009; 379: 691-695.

[54] Shekarabi M, Girard N, Riviere JB, Dion P, Houle M, Toulouse A, Lafreniere RG, Vercauteren F, Hince P, Laganiere J, Rochefort D, Faivre L, Samuels M and Rouleau GA. Mutations in the nervous system--specific HSN2 exon of WNK1 cause hereditary sensory neuropathy type II. J Clin Invest 2008; 118: 2496-2505.

[55] Zhang Z, Xu X, Zhang Y, Zhou J, Yu Z and He C. LINGO-1 interacts with WNK1 to regulate nogo-induced inhibition of neurite extension. J Biol Chem 2009; 284: 15717-15728.

[56] Goemaere J and Knoops B. Peroxiredoxin distribution in the mouse brain with emphasis on neuronal populations affected in neurodegenerative disorders. J Comp Neurol 2012; 520: 258-280.

[57] Cumming RC, Dargusch R, Fischer WH and Schubert D. Increase in expression levels and resistance to sulfhydryl oxidation of peroxiredoxin isoforms in amyloid beta-resistant nerve cells. J Biol Chem 2007; 282: 30523-30534.

[58] Sanchez-Font MF, Sebastia J, Sanfeliu C, Cristofol R, Marfany G and Gonzalez-Duarte R. Peroxiredoxin 2 (PRDX2), an antioxidant enzyme, is under-expressed in Down syndrome fetal brains. Cell Mol Life Sci 2003; 60: 1513-1523.

[59] Kim SH, Fountoulakis M, Cairns N and Lubec G. Protein levels of human peroxiredoxin subtypes in brains of patients with Alzheimer's disease and Down syndrome. J Neural Transm Suppl 2001; 223-235.

[60] Mandel S, Grunblatt E, Riederer P, Amariglio N, Jacob-Hirsch J, Rechavi G and Youdim MB. Gene expression profiling of sporadic Parkinson's disease substantia nigra pars compacta reveals impairment of ubiquitin-proteasome subunits, SKP1A, aldehyde dehydrogenase, and chaperone HSC-70. Ann N Y Acad Sci 2005; 1053: 356-375.

[61] Fishman-Jacob T, Reznichenko L, Youdim MB and Mandel SA. A sporadic Parkinson disease model via silencing of the ubiquitin-proteasome/E3 ligase component SKP1A. J Biol Chem 2009; 284: 32835-32845.

[62] Kondo S, Tanaka Y, Kondo Y, Hitomi M, Barnett

GH, Ishizaka Y, Liu J, Haqqi T, Nishiyama A, Villeponteau B, Cowell JK and Barna BP. Antisense telomerase treatment: induction of two distinct pathways, apoptosis and differentiation. FASEB J 1998; 12: 801-811.

[63] Sola S, Xavier JM, Santos DM, Aranha MM, Morgado AL, Jepsen K and Rodrigues CM. p53 interaction with JMJD3 results in its nuclear distribution during mouse neural stem cell differentiation. PLoS One 2011; 6: e18421.

[64] Lu TZ, Quan Y and Feng ZP. Multifaceted role of heat shock protein 70 in neurons. Mol Neurobiol 2010; 42: 114-123.

[65] Turturici G, Sconzo G and Geraci F. Hsp70 and its molecular role in nervous system diseases. Biochem Res Int 2011; 2011: 618127.

[66] Hoshino T, Murao N, Namba T, Takehara M, Adachi H, Katsuno M, Sobue G, Matsushima T, Suzuki T and Mizushima T. Suppression of Alzheimer's disease-related phenotypes by expression of heat shock protein 70 in mice. J Neurosci 2011; 31: 5225-5234.

[67] Salminen A, Ojala J, Kaarniranta K, Hiltunen M and Soininen H. Hsp90 regulates tau pathology through co-chaperone complexes in Alzheimer's disease. Prog Neurobiol 2011; 93: 99-110.

[68] Kins S, Crameri A, Evans DR, Hemmings BA, Nitsch RM and Gotz J. Reduced protein phosphatase 2A activity induces hyperphosphorylation and altered compartmentalization of tau in transgenic mice. J Biol Chem 2001; 276: 38193-38200.

[69] Kraus A, Groenendyk J, Bedard K, Baldwin TA, Krause KH, Dubois-Dauphin M, Dyck J, Rosenbaum EE, Korngut L, Colley NJ, Gosgnach S, Zochodne D, Todd K, Agellon LB and Michalak M. Calnexin deficiency leads to dysmyelination. J Biol Chem 2010; 285: 18928-18938.

[70] Coe H, Bedard K, Groenendyk J, Jung J and Michalak M. Endoplasmic reticulum stress in the absence of calnexin. Cell Stress Chaperones 2008; 13: 497-507.

[71] Takizawa T, Tatematsu C, Watanabe K, Kato K and Nakanishi Y. Cleavage of calnexin caused by apoptotic stimuli: implication for the regulation of apoptosis. J Biochem 2004; 136: 399-405.

[72] Jakobsson J, Cordero MI, Bisaz R, Groner AC, Busskamp V, Bensadoun JC, Cammas F, Losson R, Mansuy IM, Sandi C and Trono D. KAP1-mediated epigenetic repression in the forebrain modulates behavioral vulnerability to stress. Neuron 2008; 60: 818-831.

[73] Gelebart P, Opas M and Michalak M. Calreticulin, a Ca2+-binding chaperone of the endoplasmic reticulum. Int J Biochem Cell Biol 2005; 37: 260-266.

[74] Michalak M, Groenendyk J, Szabo E, Gold LI and Opas M. Calreticulin, a multi-process calcium-buffering chaperone of the endoplasmic reticulum. Biochem J 2009; 417: 651-666.

[75] Gold LI, Eggleton P, Sweetwyne MT, Van Duyn LB, Greives MR, Naylor SM, Michalak M and Murphy-Ullrich JE. Calreticulin: non-endoplasmic reticulum functions in physiology and disease. FASEB J 2010; 24: 665-683.

[76] Wilhelmus MM, Verhaar R, Andringa G, Bol JG, Cras P, Shan L, Hoozemans JJ and Drukarch B. Presence of tissue transglutaminase in granular endoplasmic reticulum is characteristic of melanized neurons in Parkinson's disease brain. Brain Pathol 2011; 21: 130-139.

[77] Lai CS, Preisler J, Baum L, Lee DH, Ng HK, Hugon J, So KF and Chang RC. Low molecular weight Abeta induces collapse of endoplasmic reticulum. Mol Cell Neurosci 2009; 41: 32-43.

[78] Kudo T, Kanemoto S, Hara H, Morimoto N, Morihara T, Kimura R, Tabira T, Imaizumi K and Takeda M. A molecular chaperone inducer protects neurons from ER stress. Cell Death Differ 2008; 15: 364-375.

[79] Coe H, Jung J, Groenendyk J, Prins D and Michalak M. ERp57 modulates STAT3 signaling from the lumen of the endoplasmic reticulum. J Biol Chem 2010; 285: 6725-6738.

[80] Chichiarelli S, Gaucci E, Ferraro A, Grillo C, Altieri F, Cocchiola R, Arcangeli V, Turano C and Eufemi M. Role of ERp57 in the signaling and transcriptional activity of STAT3 in a melanoma cell line. Arch Biochem Biophys 2010; 494: 178-183.

[81] Kim-Han JS and O'Malley KL. Cell stress induced by the parkinsonian mimetic, 6-hydroxydopamine, is concurrent with oxidation of the chaperone, ERp57, and aggresome formation. Antioxid Redox Signal 2007; 9: 2255-2264.

[82] Sklan EH, Podoly E and Soreq H. RACK1 has the nerve to act: structure meets function in the nervous system. Prog Neurobiol 2006; 78: 117-134.

[83] Johnson JA and Ogbi M. Targeting the F1Fo ATP Synthase: Modulation of the Body's Powerhouse and Its Implications for Human Disease. Curr Med Chem 2011; 18: 4684-4714.

[84] Sa Q, Wang Y, Li W, Zhang L and Sun Y. The promoter of an antifungal protein gene from Gastrodia elata confers tissue-specific and fungus-inducible expression patterns and responds to both salicylic acid and jasmonic acid. Plant Cell Rep 2003; 22: 79-84.

[85] Liu W, Hu YL, Wang M, Xiang Y, Hu Z and Wang DC. Purification, crystallization and preliminary X-ray diffraction analysis of a novel mannose-binding lectin from Gastrodia elata with antifungal properties. Acta Crystallogr D Biol Crystallogr 2002; 58: 1833-1835.